Proceedings of the 21st ICSMGE, Vienna, Austria, 14 – 19 June 2026. Pistrol, Adam & Schweiger (eds.)
Published by: ÖGG, Austrian Society for Geomechanics, Salzburg, Austria, ISBN 978-3-9503898-4-5
https://doi.org/10.53243/ICSMGE2026-1250

Effect of the adopted constitutive relationship on the modelling of post-liquefaction reconsolidation

Shengjie Ma, David M.G. Taborda
Department of Civil and Environmental Engineering, Imperial College London, United Kingdom, s.ma22@imperial.ac.uk

Stavroula Kontoe
Department of Civil Engineering, University of Patras, Greece; Department of Civil and Environmental Engineering, Imperial College London, London, United Kingdom

ABSTRACT: Ground settlement is one of the main consequences of liquefaction and can develop during seismic shaking, as well as for a period after the end of the strong motion. In the post-shaking phase, once the seismic shaking ceases, water continues to flow upwards towards the surface, with ground settlement evolving until the excess pore water pressure is completely dissipated within the soil deposit. This process, known as post-liquefaction reconsolidation or simply reconsolidation, results in volumetric strains and settlements, which are challenging to model numerically using conventional constitutive frameworks for sands as loading under constant stress-ratio is often not captured accurately. In this study, a modified bounding surface plasticity model employing four different elastic stiffness constitutive relationships is proposed to improve the accuracy of simulating post-liquefaction reconsolidation. Fully coupled dynamic consolidation finite element analyses of level ground deposits subjected to seismic loading are conducted, illustrating the impact of the new formulation in terms of excess pore pressure dissipation and ground settlement evolution.

KEYWORDS: Post-liquefaction reconsolidation; co-seismic phase; post-shaking phase; liquefaction; fully coupled simulation.

1 INTRODUCTION

Earthquake-induced liquefaction takes place when excess pore pressure reaches the initial effective vertical stress of the liquefiable saturated soil, owing to the soil's contractive behaviour when subjected to seismic loading. Driven by this elevated pore pressure (hydraulic gradient) during and after the seismic shaking, water in the soil pores migrates upwards towards the ground surface, which typically is the only drainage boundary, allowing water to seep out of the deposit. During this process, the evolution of pore pressures and the development of volumetric strains, which inevitably lead to ground settlements, can occur simultaneously (Adamidis & Madabhushi 2016; Adamidis & Madabhushi 2018; Ma et al. 2025), involving partially drained conditions.

Ma et al. (2025) analysed eight well-documented free-field dynamic centrifuge tests and confirmed that ground settlements occur primarily during the co-seismic phase where the earthquake loading is applied and liquefaction takes place. However, finite element analyses with advanced constitutive models often underpredict volumetric strains that develop throughout the soil profile (i.e., settlement) and struggle to capture accurately the evolution of excess pore pressure during and after seismic shaking (Arulanandan and Sybico 1992; Taiebat et al. 2007; Ma et al. 2023; Ma et al. 2024). This is partly due to the underestimation of the hydraulic conductivity during the co-seismic phase and partly due to modelling challenges in terms of reproducing stiffness in the post-shaking phase. Ma et al. (2025) proposed a new back-analysis methodology to quantify the variation of hydraulic conductivity during liquefaction and found that this property increases significantly at the onset of liquefaction and then gradually decreases to its initial value, prior to the seismic shaking. The volumetric strains will be particularly affected from the variations of hydraulic conductivity. Increasing the hydraulic conductivity during liquefaction can improve the accuracy of both the predicted rate and magnitude of ground settlements, but it can lead to larger discrepancies in the prediction of excess pore pressure (Ma et al. 2023). In addition to the hydraulic conductivity, the volumetric stiffness, either quantified by the bulk modulus or, under one-dimensional conditions, by the constrained modulus, also plays a key role, governing the dissipation rate of excess pore pressure and the corresponding magnitude of post-liquefaction reconsolidation. Several studies have attempted to identify experimentally the stiffness of saturated soil at low effective stress or during post-liquefaction reconsolidation (Brennan & Madabhushi 2011; Haigh et al. 2012; Zeybek & Madabhushi 2023). However, it is still challenging to predict accurately both ground settlements and excess pore pressures using conventional constitutive relationships. As an important step towards improving the accuracy of earthquake-induced liquefaction modelling, the effect of the adopted volumetric stiffness on the simulation of post-liquefaction reconsolidation requires investigation.

In this study, four alternative volumetric stiffness constitutive relationships are incorporated into the bounding surface plasticity constitutive model IC MAGE M14 (Taborda, 2011; Taborda et al. 2014), which is implemented in PLAXIS as a user-defined soil model (Moller et al. 2025). Effective stress analyses, with a fully coupled $(u-p)$ dynamic consolidation formulation, are carried out in PLAXIS (Bentley Systems, 2024) to replicate a free-field dynamic centrifuge test VELACS model No.1 (Arulmoli et al. 1992; Arulanandan & Scott 1993). The numerically predicted responses are evaluated against excess pore pressures and ground settlement measured in the centrifuge to assess the performance of each constitutive relationship.

2 NUMERICAL MODELLING

2.1 *Brief description of VELACS model No.1*

The free-field dynamic centrifuge test VELACS model No.1 adopted in this study was conducted within the Verification of Liquefaction Analyses by Centrifuge Studies (VELACS) project (Arulmoli et al. 1992; Arulanandan & Scott 1993). In this dynamic centrifuge test, the laminar box is composed of various rings of negligible mass and interface friction (see Figure 1). The soil deposit in this laminar box is comprised of fully saturated Nevada sand with hydraulic conductivity of 6.583×10^{-5} m/s, measured under 1g conditions. Water was used as the saturation fluid in the centrifuge test, while 50g gravity acceleration is employed for simulating the actual stress state during and after the seismic shaking. As a result, the real hydraulic conductivity under the 50g gravity acceleration is 50 times larger than that measured under 1g conditions. Two linear

variable differential transformers (LVDTs) were installed at the surface, while two sets of pore pressure transducers were located at different elevations (-1.45m, -2.6m, -5.0m, and -7.5m). It should be noted that in this study all numerical simulations are conducted in prototype scale, and all dimensions or dynamic responses are also in prototype scale. The dynamic centrifuge test can be simulated by a plane strain soil column with tied degrees of freedom at the lateral sides (see Figure 1). In terms of hydraulic boundary conditions, the base and the lateral sides are impermeable, with seepage only allowed at the surface of the soil column. The motion used in this test consisted of 20 loading cycles with a frequency of roughly 2 Hz and a maximum horizontal acceleration of 2 m/s^2.

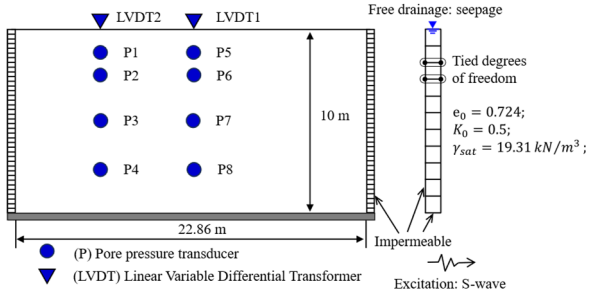

Figure 1. Side view of VELACS Model No.1 in prototype scale and the corresponding numerical model setups.

2.2 *IC MAGE M14 constitutive model*

The mechanical behaviour of saturated sand subjected to seismic loading is modelled with the IC MAGE M14 (Taborda, 2011; Taborda et al., 2014; Moller et al. 2025), using the IC MAGE UMIP framework (Taborda et al. 2024b). This model is based on the formulation proposed by Papadimitriou & Bouckovalas (2002), itself a modified version of the original bounding surface plasticity framework proposed by Manzari & Dafalias (1997), with several enhancements introduced by Taborda (2011) and Taborda et al (2014), including a power-law formulation for the critical state line, a modified hardening modulus, and a second yield surface. IC MAGE M14 can model the contraction and dilatancy of sand materials both under monotonic and cyclic loading conditions, requiring the definition of up to 34 material parameters, all of which are explained in detail in Taborda (2011), Taborda et al. (2014) and Moller et al. (2025). The main objective of this study is to investigate the effect of the adopted constitutive relationships in terms of volumetric stiffness on the modelling of post-liquefaction reconsolidation, so only the elastic behaviour part of M14 will be described in detail.

2.3 *Shear stiffness*

In the constitutive model IC MAGE M14, the shear stiffness of the material is calculated by:

$$G_{\tan} = \frac{G_{\max}}{T} \geq \mathrm{G_{min}} = \frac{G_{\max}}{1 + \kappa \cdot \left(\frac{1}{a_1} - 1\right)} \tag{1}$$

$$G_{\max} = B_G \cdot f(e) \cdot p_{\mathrm{ref}}^{\prime(1-n_S)} \cdot p^{\prime(n_S)} \tag{2}$$

$$f(e) = \frac{1}{0.3 + 0.7 \cdot e^2} \tag{3}$$

where p' is the mean effective stress; n_s is the parameter determining the nonlinearity of the stress-dependency of the shear modulus; p'_{ref} is the reference pressure; $f(e)$ is the void ratio-dependency function and e is the current void ratio. In this study, Equation (3) is always adopted to determine $f(e)$.

In Equation (1), the reduction factor T is given by:

$$T = 1 + \kappa \cdot \left(\frac{1}{a_1} - 1\right) \cdot \left(\frac{\sqrt{\frac{1}{2} \cdot (\boldsymbol{r} - \boldsymbol{r}^{\mathbf{SR}}) : (\boldsymbol{r} - \boldsymbol{r}^{\mathbf{SR}})}}{N_{\mathrm{T}} \cdot \left(a_1 \cdot \left(\frac{G_{\max}^{\mathrm{SR}}}{p'^{\mathrm{SR}}}\right) \cdot \gamma_1\right)} \right)^{\kappa - 1} \tag{4}$$

where a_1, γ_1 and κ are model parameters (see Taborda et al. (2014)); p'^{SR} is the mean effective stress at the last shear reversal and $G_{\max}^{\mathrm{SR}}$ is the corresponding maximum shear modulus; N_T is a hardening parameter introducing the Masing rules, which is initialised as 1 and changes to 2 once a shear reversal is detected; $\boldsymbol{r}$ and $\boldsymbol{r}^{\mathbf{SR}}$ are stress ratio tensors calculated by Equation (5), where $\boldsymbol{s}$ is the deviatoric stress tensor and $\boldsymbol{I}$ is the identity tensor. Reversal detection is defined using and analogous formulation based on the deviatoric strain tensor (see Taborda (2011) for details).

$$\boldsymbol{r} = \frac{\boldsymbol{s}}{p'} = \frac{\boldsymbol{\sigma}' - p' \cdot \boldsymbol{I}}{p'} \tag{5}$$

2.4 *Volumetric stiffness*

As mentioned earlier, the main modifications introduced in M14 for this study (Moller et al. 2025) involve the inclusion of four volumetric stiffness formulations that influence not only the accumulation of excess pore pressure but also the associated ground settlements. These formulations are presented in the following sections.

2.4.1 *Constant Poisson's ratio*

In this case, the bulk stiffness K_{tan} is determined by Hooke's law, which is directly associated with the shear stiffness G_{tan} (see Equation (1)) through a Poisson's ratio ν:

$$K_{\tan} = \frac{2 \cdot (1 + \nu)}{3 \cdot (1 - 2 \cdot \nu)} \cdot G_{\tan} \tag{6}$$

2.4.2 *Stress-dependent bulk modulus*

The bulk stiffness is defined using a hypoelastic formulation similar to that used for the maximum shear modulus (Equation (2)), without considering any reduction of shear stiffness:

$$K_{\max} = B_K \cdot f(e) \cdot p_{\mathrm{ref}}^{\prime(1-n_S)} \cdot p^{\prime(n_S)} \tag{7}$$

where B_K is the bulk modulus coefficient. Since no reduction of bulk modulus is considered in this formulation, $K_{\max} = K_{tan}$.

2.4.3 *Stress-dependent constrained modulus*

In this version, the second elastic constant is assumed to be the constrained modulus M_{tan}, given by a hypoelastic formulation analogous to that used for the maximum shear modulus in Equation (2), disregarding any possible reduction of shear stiffness:

$$M_{\tan} = B_M \cdot f(e) \cdot p_{\mathrm{ref}}^{\prime(1-n_S)} \cdot p^{\prime(n_S)} \tag{8}$$

where B_M is the constrained modulus coefficient. For comparison purposes, the resulting bulk modulus can be calculated using Hooke's law:

$$K_{\tan} = M_{\tan} - \frac{4G_{\tan}}{3} \tag{9}$$

2.4.4 *Constant swelling line*

Assuming a swelling line of constant slope κ_{iso} in $e - \ln p'$ space, the bulk modulus can be calculated using:

$$K_{\tan} = \frac{(1 + e) \cdot p'}{\kappa_{iso}} \tag{10}$$

2.5 *Model parameters*

The input parameters for Nevada sand used in the VELACS model No.1 can be found in Taborda et al. (2014). Four different numerical simulations of VELACS model No.1 are carried out employing different stiffness formulations as listed in Table 1. It should be noted that, with the exception of volumetric stiffness parameters, in these four models, all other parameters of Nevada sand utilised are the same as Taborda et al. (2014). For Model 1, the original formulation of constant Poisson's ratio $\upsilon = 0.2$ is used; for Model 2, the average value between $G_{\max}$ and $G_{\min}$ in Equation (1) is calculated and converted into the corresponding bulk modulus using $\upsilon = 0.2$. This yields a parameter $B_K = 406.7$ to use in Equation (7). The same process is repeated for the constrained modulus in Model 3, resulting in $B_M = 813.5$. This implies that, for a certain level of reduction in shear modulus, the three models (1, 2 and 3) all have the same elastic properties. Lastly, in Model 4, the swelling index, κ_{iso}, is calibrated based on the results of oedometer tests on Nevada sand from the VELACS project (Arulmoli et al. 1992; Arulanandan & Scott 1993).

Table 1. Bulk stiffness used for different models.

Case ID	Bulk stiffness	Parameters	Equations
Model 1	Constant Poisson's ratio	υ=0.2	(6)
Model 2	Stress-dependent bulk modulus	B_K=406.7	(7)
Model 3	Stress-dependent constrained modulus	B_M=813.5	(8) (9)
Model 4	Constant swelling line	κ_{iso}=0.0041	(10)

3 VARIABLE PERMEABILITY MODEL

Hydraulic conductivity changes significantly during and after liquefaction (Haigh et al. 2012; Ma et al. 2025). To account for the variable hydraulic conductivity, this study employs the variable permeability model IC MAGE Flow Model 03 (Taborda et al. 2024a), implemented into PLAXIS as a User-Defined Flow Model. Its formulation adopts the mean effective stress ratio r_p introduced by Tsaparli et al. (2020) based on Taborda (2011):

$$\frac{k}{k_0} = 1 + \left(\frac{k_{\max}}{k_0} - 1\right) \times \left(\frac{r_p}{r_{pl}}\right)^n \quad (11)$$

where the mean effective stress ratio is defined according to $r_p = \Delta p'/p'_0$; $\Delta p'$ is the change in mean effective stress since the start of the analysis and p'_0 is the initial mean effective stress level, i.e. prior to the application of the dynamic loading; k_0 is the initial static permeability; k_{max}/k_0 represents the ratio between the liquefied permeability and the static permeability; n denotes the nonlinear parameter that controls the rate of permeability increase; r_{pl} designates the pore pressure ratio at which the liquefaction takes place. As this model is r_p-based, it will not be affected by changes in total stress, meaning it is also applicable to simulations involving bi-directional seismic loading. In this study, all the presented analyses adopted the following parameters for the variable permeability model: $k_{max}/k_0 = 10$, $n = 10$, $r_{pl} = 0.9$, $k_0 = 3.292 \times 10^{-3}$ m/s, as adopted in Tsaparli et al. (2020).

4 NUMERICAL RESULTS

The dynamic response in terms of ground settlement during the co-seismic and post-shaking phases is illustrated in Figure 2. Clearly, as postulated by Ma et al. (2025), the adoption of a variable permeability model that can capture the effects of increased pore water pressure during the co-seismic phase, leads to a substantial improvement in terms of simulating the rate of settlement, with the obtained results using the four formulations being very close to the observed behaviour. It is interesting to note that Models 1, 2 and 3 lead to very similar responses. This suggests that, while the tangent shear stiffness $G_{\tan}$ varies considerably due to shearing, the adoption of an average value of this property appears to be representative of the behaviour calculated during the entire analysis. Conversely, Model 4, which adopts an entirely different description for the volumetric stiffness, shows a slightly improved response, with a constant rate of settlement being observed during the seismic phase and slightly larger settlements being obtained during the post-shaking phase (roughly from $12.5\ s$ onwards).

Given that an additional objective is to compare the impact of the different formulations on the reconsolidation behaviour, the pore pressure time histories during the post-shaking phase are analysed in detail. A direct comparison is difficult since the volumetric elastic stiffness impacts on the generation of excess pore pressure during undrained loading. This is further complicated by the use of the variable permeability model: as pore pressure rises, the mean effective stress reduces and the permeability increases, further reducing the pore pressure. Therefore, to isolate the effect of the adopted volumetric stiffness, Figure 3 shows the excess pore pressure time histories, $u_e(t)$, normalised by the excess pore pressure at the start of the post-shaking phase, i.e. $u_e(t = 12.5\ s)$. It should be noted that, despite the abovementioned mechanisms, the differences between the values of $u_e(t = 12.5\ s)$ are relatively small. Clearly, the results mirror those of the settlement time histories, with Models 1, 2 and 3 showing, in general, good agreement between them, particularly from $t = 2\ s$ onwards. Up to this point, there are some discernible differences, possibly due to residual oscillations in the soil deposit. Model 4 shows a very distinctive behaviour, with pore pressures remaining at a higher level for longer. In this post-shaking phase, the use of the variable permeability model leads to slightly unrealistic results as it artificially accelerates the dissipation of pore pressures (see Figure 3). This can be understood by considering the observations made by Ma et al. (2025), according to which the permeability should reduce to its 'static' value once shaking stops, in these analyses the permeability retains high values, as long as pore pressures remain elevated and independently of whether shaking has stopped. The adoption of a different hydraulic model that can mimic the behaviour identified in Ma et al. (2025) would certainly have resulted in a different pattern being observed.

5 CONCLUSIONS

In this paper, the performance of a modified bounding surface plasticity model employing four different constitutive relationships for the volumetric stiffness is explored together with a variable permeability model for simulating liquefaction. Emphasis is placed on quantifying the effect of the volumetric stiffness in terms of ground settlements during the co-seismic and post-shaking phases, as well as on post-liquefaction reconsolidation. The results show that, independently of the adopted formulation, the use of a variable permeability model significantly improves the prediction of co-seismic settlement. However, in the post-shaking phase, the link between excess pore pressure and permeability introduced by the hydraulic model leads to faster pore pressure dissipation than expected.

The adoption of a constant swelling index as a representation of the volumetric stiffness, which can be calibrated directly from oedometer tests, resulted in better settlements and slower pore pressure dissipation during the

post-shaking phase. Clearly, results show that accurate representation of volumetric stiffness during the entire time-history in liquefied soils is important, as it governs both pore pressure build-up and post-liquefaction reconsolidation.

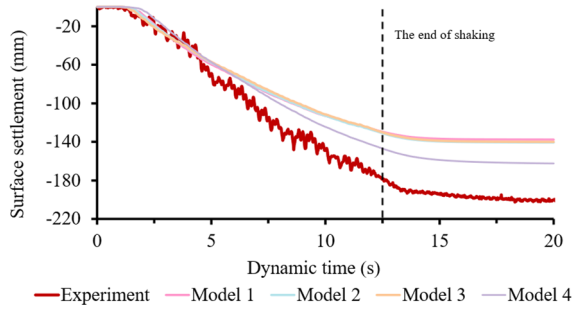

Figure 2. Settlements time-histories for different models.

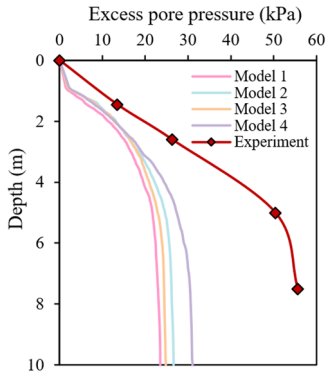

Figure 3. Excess pore water pressure profile at time point of 12.5s

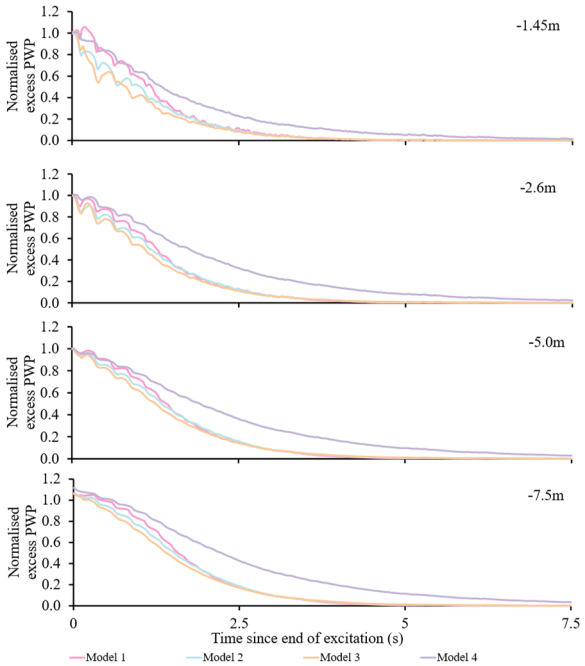

Figure 4. Normalised excess pore water pressure (pwp) for different models.

6 ACKNOWLEDGEMENTS

The authors gratefully acknowledge the Dixon Scholarship awarded to the first author by the Department of Civil and Environmental Engineering, Imperial College London.

7 REFERENCES

Adamidis, O. and Madabhushi, G.S.P., 2016. Post-liquefaction reconsolidation of sand. *Proceedings of the Royal Society A: Mathematical, Physical and Engineering Sciences*, 472(2186), p.20150745.

Adamidis, O. and Madabhushi, S.P.G., 2018. Experimental investigation of drainage during earthquake-induced liquefaction. *Géotechnique*, 68(8), pp.655-665.

Arulanandan, K. and Sybico Jr, J., 1992. Post-liquefaction settlement of sands. *In Predictive soil mechanics: Proceedings of the Wroth Memorial Symposium held at St Catherine's College*, Oxford, 27-29 July 1992 (pp. 94-110). Thomas Telford Publishing.

Arulanandan, K., and Scott, R. F. 1993. Verification of numerical procedures for the analysis of soil liquefaction problems. *Proceedings of the International Conference on the Verification of Numerical Procedures for the Analysis of Soil Liquefaction Problems*.

Arulmoli K, Muraleetharan KK, Hossain MM, Fruth LS. 1992. VELACS: verification of liquefaction analyses by centrifuge studies - laboratory testing program and soil data report. Earth Technology Project No. 90-0562.

Bentley Systems., 2024. CONNECT Edition V24.03 PLAXIS 2D - Reference Manual.

Brennan, A.J. and Madabhushi, S.P.G., 2011. Measurement of coefficient of consolidation during reconsolidation of liquefied sand. *Geotechnical Testing Journal*, 34(2), pp.139-146.

Haigh, S.K., Eadington, J. and Madabhushi, S.P.G., 2012. Permeability and stiffness of sands at very low effective stresses. *Géotechnique*, 62(1), pp.69-75.

Ma, S., Kontoe, S. and Taborda, D.M.G., 2023. On the impact of soil permeability in the numerical simulation of seismically induced liquefaction. *In Proceedings of the 10th European Conference on Numerical Methods in Geotechnical Engineering, NUMGE2023*. International Society for Soil Mechanics and Geotechnical Engineering. DOI: https://doi.org/10.53243/NUMGE2023-406

Ma, S., Kontoe, S., Taborda, D.M.G., 2024. Layered system response effects of liquefiable deposits. *Japanese Geotechnical Society Special Publication*, 10(23), pp.848-853.

Ma, S., Kontoe, S. and Taborda, D.M.G., 2025. Quantifying the variation of hydraulic conductivity during seismic liquefaction. *Soil Dynamics and Earthquake Engineering*, 197, p.109518.

Manzari, M.T. and Dafalias, Y.F. 1997: A critical state two-surface plasticity model for sands. *Geotechnique*, 47(2), 255-272.

Moller, JK, Ma, S, Taborda, DMG. 2025. IC MAGE Model 14 – bounding surface plasticity model for sands under static and cyclic loading (Version 1.4). *Zenodo*. doi: 10.5281/zenodo.16875962

Papadimitriou, A.G. and Bouckovalas, G.D. 2002. Plasticity model for sand under small and large cyclic strains: a multiaxial formulation. *Soil Dynamics and Earthquake Engineering*, 22(3), pp.191-204.

Taborda, D.M.G, Kontoe, S., Ma, S., 2024a. IC MAGE Flow Model 03 – Variable permeability model for simulating liquefaction. *Zenodo*. doi: 10.5281/zenodo.10496632

Taborda, D.M.G., 2011. Development of constitutive models for application in soil dynamics, *Ph.D. thesis*, Imperial College London, London.

Taborda, D.M.G., Zdravković, L., Kontoe, S. and Potts, D.M. 2014. Computational study on the modification of a bounding surface plasticity model for sands. *Computers and Geotechnics*, 59, pp.145-160.

Taborda, DMG, Kontoe, S, Tsiampousi, A. 2024b. IC MAGE UMIP – universal model interface for PLAXIS (Version 3.6). *Zenodo*. doi: 10.5281/zenodo.13890543

Taiebat, M., Shahir, H. and Pak, A., 2007. Study of pore pressure variation during liquefaction using two constitutive models for sand. *Soil Dynamics and Earthquake Engineering*, 27(1), pp.60-72.

Tsaparli, V., Kontoe, S., Taborda, D.M.G. and Potts, D.M., 2020. A case study of liquefaction: demonstrating the application of an advanced model and understanding the pitfalls of the simplified procedure. *Géotechnique*, 70(6), pp.538-558.

Zeybek, A. and Madabhushi, G.S.P. 2023. Assessment of soil parameters during post-liquefaction reconsolidation of loose sand. *Soil Dynamics and Earthquake Engineering*, 164, p.107611.